Application Notes

Multisine Signals for Wireless System Test and Design

■ **Nuno B. Carvalho, Kate A. Remley, Dominique Schreurs, and Kevin G. Gard**

Multisine signals are used in the laboratory and in the field to provide a periodic, well-characterized waveform that can simulate complex modulated radio frequency (RF) signals. For example, in the field of wireless telecommunications, multisines are often used to provide realistic test signals that have statistics similar to various types of digitally modulated signals. Multisines are used for system testing [1]–[3], for verifying technology standard masks [4]–[6], and more and more for device and system modeling [7]–[12] in order to extract robust models for computer-aided design/computer-aided engineering (CAD/CAE) solutions. Recently, their use as calibration signals is also being explored [13], [14].

It was not so long ago that practical communication signals had small enough amplitude variations and were narrowband enough that simple two-tone test signals were sufficient to characterize the nonlinearity of wireless system components. Two-tone test signals have been extremely popular for nonlinear characterization because they are conceptually straightforward to understand and use in analytic descriptions of nonlinear circuits. Indeed, many fundamental concepts regarding nonlinear circuit response, such as intermodulation distortion, cross-modulation, memory effects [15], and gain compression/expansion, are clearly illustrated by the use of two-tone test signals. Unfortunately, the amplitude, phase, and bandwidth characteristics of modern wireless signals can no longer

be accurately represented by a simple two-tone test signal. The digital cellular and wireless local area network (WLAN) signals of today are wideband and contain significant amplitude variations as a byproduct of implementing high-spectral-efficiency modulation schemes to increase the amount of data transmitted for a fixed amount of bandwidth.

In general, the best signals to use in laboratory testing are those that exactly match the signal that will be input to the system in real operation, or those that place the system into a wide variety of operating states. One commonly used signal in this category is white Gaussian noise (WGN). However, this nonperiodic signal has a continuous spectrum that is difficult to generate and measure using instruments designed to measure bandpass signals. This is one reason why test signals such as multisines are gaining importance in the world of instrumentation and measurement, because they can be generated and recorded very efficiently for systematic measures.

Multisines consist of a sum of several simultaneously generated sinusoids (tones). Equation (1) presents a typical multisine signal:

$$x(t) = \sum_{k=1}^{N} A_k \cos(\omega_k t + \theta_k),\qquad (1)$$

where A_k is the amplitude and θ_k is the phase of the kth sinusoid, N is the number of sinusoids, and $\omega_k = \omega_0 + (k-1)\Delta\omega$, with ω_0 being the frequency of the first tone and $\Delta\omega$ the constant frequency separation between them.

By changing the relative phase between each of the frequency components in the multisine, we are able to change the time-domain envelope associated with the multisine. "Defining Relative Phase in a Multisine Signal" illustrates

Nuno B. Carvalho is with the University of Aveiro. Kate A. Remley is with the National Institute of Standards and Technology. Dominique Schreurs is with Katholieke Universiteit Leuven. Kevin G. Gard is with North Carolina State University.

Defining Relative Phase in a Multisine Signal

Relative phase for a signal consisting only of a fundamental and harmonics is a straightforward quantity to understand and calculate. Using the fundamental tone as a reference, we compute the difference in phase between this reference and all other harmonically related phases measured at a given instant. Because the frequency components are harmonically related, we can always find the difference in phase no matter at what point in the waveform we collect our sample.

Relative phase as it relates to the nonharmonically related components in a multisine is somewhat more complicated. (In fact, these components are also harmonically related as integer multiples of $\Delta\omega$; however, we do not typically measure all of these components when we are measuring a bandpass signal.)

It is easiest to understand the concept of relative phase for a multisine in the time domain. At each point in the time-domain envelope signal, the phase relationships between the frequency components of a multisine are different, as illustrated in Figure A. Here we see a three-tone multisine whose frequency components were specified to have zero-degree relative phases. At time $t = t_{ref}$, when the multisine was generated, this phase relationship holds. However, at other times in the envelope time period, other vastly different phase relationships occur.

Thus, we need to understand that when a multisine is specified to have a given phase relationship between its tones, this relationship will only hold at integer multiples of the envelope period relative to the reference time. And, more importantly, since we will typically measure this waveform at some random time in the envelope, we will have to find a way to determine the reference time. Various techniques exist for carrying out this alignment either in postprocessing [30] or during the measurement.

The concept of relative phase alignment in a multisine can be extended to distortion products as well. By sampling the input and output waveforms at the same instant, and determining the time in the waveform that best fits the specified phase values, we can read off the phase of output frequency components, including intermodulation products, directly. Figure B shows an example of a two-tone excitation signal and a third-order intermodulation prod-
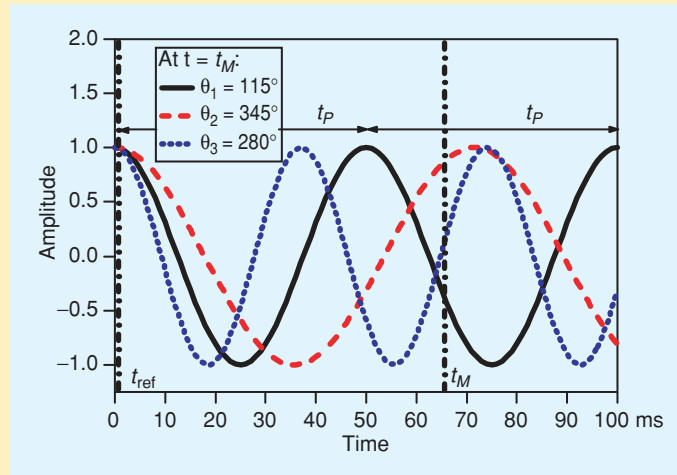

Figure A. *This three-tone multisine was generated with relative phases of 0°. However, the phases may appear different from zero depending on when the waveform is sampled. For example, if the waveform is sampled at time $t = t_M$, the phases have values of 115°, 345°, and 280° [30].*
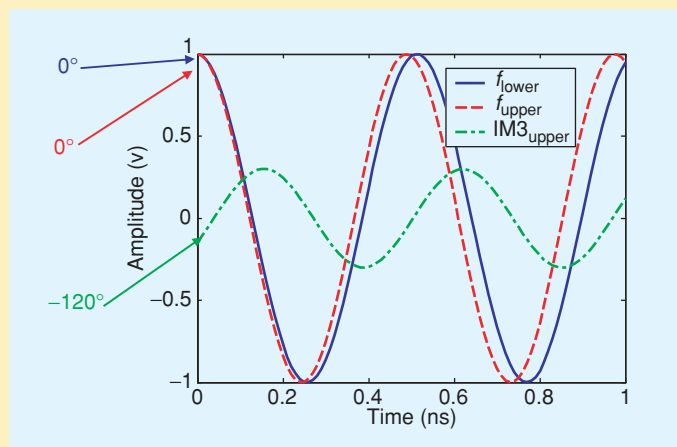

Figure B. *The relative phase of an intermodulation product can be found by measuring the output waveform at the same instant as the input waveform and aligning (or detrending) the measurement to the reference time.*

uct. Once the reference time is determined (0 ns in this example), the phase of the intermodulation product relative to the specified input phases can be determined directly.

the concept of relative phase in a signal. Figure 1 presents some of the many different time-domain waveforms that can be generated depending on the relative phase and amplitude of each tone in the multisine. In this case, the power spectral density (PSD) is identical for each multisine; however, the statistics of the waveforms such as peak-to-average power ratio (PAPR) are vastly different. So, a careful design of the excitation multisine both in amplitude and phase is fundamental for correctly predicting laboratory experiments.

There are many reasons to use multisine signals in design and test. First, as mentioned above, multisines are periodic signals. Periodic signals are straightforward to generate and measure by using many instruments commonly used to characterize bandpass modulated signals such as vector signal generators, spectrum analyzers, vector signal analyzers, and large-signal network analyzers (LSNAs). In fact, some instruments such as the LSNA [16], [17] require the use of periodic excitations.

Second, it is straightforward to change the statistics of multisine signals by changing the relative phase between their components. Using algorithms such as the one presented in the "Statistical Behavior of Multisines" section, we can readily synthesize different types of excitations that can mimic digital modulations of interest.

Third, because a multisine is composed of sine waves, it is a relatively straightforward task to characterize the harmonic distortion in the excitation signal by a simple fit to ideal sine waves. Also, the relative phase between the sinusoidal frequency components is straightforward to measure and characterize, as discussed in "Defining Relative Phase in a Multisine Signal".

Finally, when carrying out common wireless system measurements such as harmonic distortion, intermodulation distortion, frequency-selective fading, or other tests where phase plays a role, knowledge of the phases at the input and output of the system under test can yield insight into distortion-causing mechanisms. The use of sine waves facilitates this.

This article first presents multisine representations using discrete Fourier transform (DFT) coefficients. We describe some of the statistical characteristics of multisines, and we present issues related to developing correct statistics and choosing the correct values of the amplitude and phase of each tone. Then, we address some of the test setups for measuring multisines and issues related to their use. Finally, we present some examples of the use of multisines to simulate digital modulation in the design and test of wireless communication systems.

Accurate Multisine Representations Using DFT Coefficients

One goal of multisine signal analysis is to extend the analytic simplicity of two-tone nonlinear system analysis to more complicated signals. However, the two questions that quick-

Multisine with Predetermined Higher-Order Statistics (continued)

Expectations such as (d) are known as the signal's higher-order statistics [11] because they can be understood as being higher-order extensions of the first-order PSD, $S_{xx}\omega$). We conclude that two signals, $x(t)$ and $x_r(t)$, are similar up to order n in the sense that they will present similar PSDs if they have similar nth-order spectra $S_{xx}(\omega) \approx S_{x_r x_r}(\omega)$, $S_{xxxx}(\omega_1, \omega_2, \omega_3) \approx S_{x_r x_r x_r}(\omega_1, \omega_2, \omega_3), \dots, S_{x\dots x}(\omega_1, \dots, \omega_{n-1}) \approx S_{x_r \dots x_r}(\omega_1, \dots, \omega_{n-1})$.

The main problem in this multisine signal design is the high number of unknowns to be matched. For instance, if the noise is sampled with $2K + 1$-points and then transformed using the DFT, $S_{xx}(\omega)$ will involve only an average made over $2K + 1$ complex numbers per signal realization. On the other hand, a second-order analysis utilizing $S_{xxxx}(\omega_1, \omega_2, \omega_3)$ already involves an average over $(2K + 1)^3$ complex entities and, for third-order analysis, $S_{x\dots x}(\omega_1, \omega_2, \omega_3, \omega_4, \omega_5)$ must be estimated from averaging complex matrices of size $(2K + 1)^5$.

This implies that the design algorithm for this type of multisine signal is extremely burdensome computationally. While, on the one hand, a lower number of sines is better for implementing the algorithm, on the other it restricts the number of unknowns and thus the number of free states.

So a better approach is to consider a large number of sines, but approximate the PSD only in selected frequency bins. In fact, this is exactly what many RF designers do when they simulate and/or measure a DUT with a large number of pseudo-random samples. Essentially, this corresponds to a large number of different multisines. Figure C presents this idea.

The design algorithm to generate this multisine consists of the optimization of the PSD of our multisine and the real signal in those bins by utilizing the higher-order statistics. For instance, for a third-order nonlinearity, the errors to be minimized are expressed in (e).
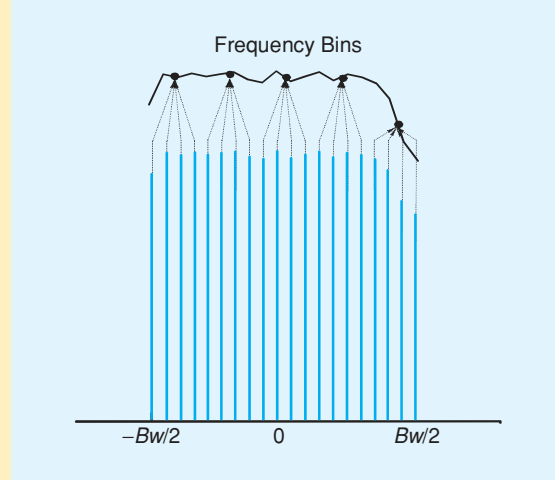

Figure C. *Original signal's PSD function and the approximating multisine matched in a certain number of predefined frequency bins [11].*

$$\varepsilon_{4,b_1,b_2,b_3} = \sum_{m_1=\frac{(b_1-1)M}{B}+1}^{\frac{b_1 M}{B}} \sum_{m_2=\frac{(b_2-1)M}{B}+1}^{\frac{b_2 M}{B}} \sum_{m_3=\frac{(b_3-1)M}{B}+1}^{\frac{b_3 M}{B}}$$

$$\times \left\{ A_{m_1} A_{m_2} A_{m_3} A_{(m_1+m_2-m_3)} e^{j\left[\phi_{m_1}\phi_{m_2}-\phi_{m_3}-\phi_{(m_1+m_2-m_3)}\right]} \right\}$$

$$- \sum_{k_1=\frac{(b_1-1)M}{B}+1}^{\frac{b_1 M}{B}} \sum_{k_2=\frac{(b_2-1)M}{B}+1}^{\frac{b_2 M}{B}} \sum_{k_3=\frac{(b_3-1)M}{B}+1}^{\frac{b_3 M}{B}}$$

$$\times E\left[X\left(\omega_{k_1}\right) X\left(\omega_{k_2}\right) X\left(\omega_{k_3}\right) * X\left(\omega_{k_1} + \omega_{k_2} - \omega_{k_3}\right)*\right] ;$$

$$b_1, b_2, b_3 \in \{1, \dots, B\} . \tag{e}$$

Reference [11] gives more information on the design of this type of multisine.

ly arise when designing multisine signals to accurately represent wireless communication signals are: 1) How many sinusoids should be used? and 2) How should the amplitude and phase of each sinusoid be determined? One straightforward approach to answering both questions is to consider a Fourier series representation of the communication signal, since it defines the signal as a sum of sinusoids. In practice, a

DFT is used to obtain Fourier series coefficients of a complex signal of finite time duration

$$x(n) = \sum_{k=0}^{N-1} A_k \cdot e^{j(2\pi kn/N + \theta_k)} = \frac{1}{N} \sum_{k=0}^{N-1} X(k) \cdot e^{j2\pi kn/N},$$

$$\tag{2}$$

where A_k and θ_k are obtained from a DFT of the desired time-domain signal. The DFT generates N Fourier coefficients for N time samples. Signal length is defined in the time domain by the end time sample minus the start time sample. This is inversely related to the frequency resolution of the DFT. The longer the signal length, the finer the frequency resolution. A simple solution to minimize the number of sinusoids is to simply remove the frequencies that are outside the bandwidth of the desired signal. In practice, the truncated bandwidth should be larger than the actual signal bandwidth by approximately 20% to minimize any error between the original signal and the truncated multisine representation of the signal [18]. The resulting signal is an accurate multisine representation of the original signal that is suitable for use in circuit simulations or laboratory measurements.

To illustrate this technique, we modeled a 163-μs reverse-link segment of a code division multiple access (CDMA) signal under the interim standard IS95A. For modulation, we used offset quadrature-phase-shift-keying (OQPSK) modulation corresponding to 200 symbols. We modeled this signal using 240 tones obtained from the DFT of a time-domain signal. The signal sampling rate was 4.9512 MHz, which is four times the information signal bandwidth. The number of necessary tones is calculated from the number of DFT tones that occur over the signal bandwidth including the 20% margin,

$$N_{\text{tones}} = \frac{1.2 \cdot f_{bw}}{f_{res}} = 1.2 \cdot f_{bw}T, \qquad (3)$$

where T is the duration of the signal being modeled. A comparison of the measured spectrum of the CDMA IS95A signal and the 240-tone multisine representation is shown in Figure 2. Note that the number of tones increases proportionally to the increase in signal length. The spectra of the two signals are nearly identical because the multisine representation was generated directly from the DFT of the time-domain signal. The one spectral feature that distinguishes one from the other is the truncated out-of-band spectral components for the multisine signal. The original CDMA signal contains spectral content outside the signal bandwidth due to the finite rejection of the baseband filters used to filter the in-phase and quadrature OQPSK datastreams. The multisine signal is truncated to just the signal bandwidth, so the out-of-band spectral components are removed. In reality, there is very little difference between the multisine representation and the time-domain representation. But that is the point of the exercise—to illustrate that a real signal can be defined by a multisine derived from the Fourier coefficients.

Our method maintains high accuracy in representing the amplitude, phase, and bandwidth characteristics of the original signal; however, there may be cases where the signal length of interest generates too many tones to be practical for circuit simulations or analytical techniques.
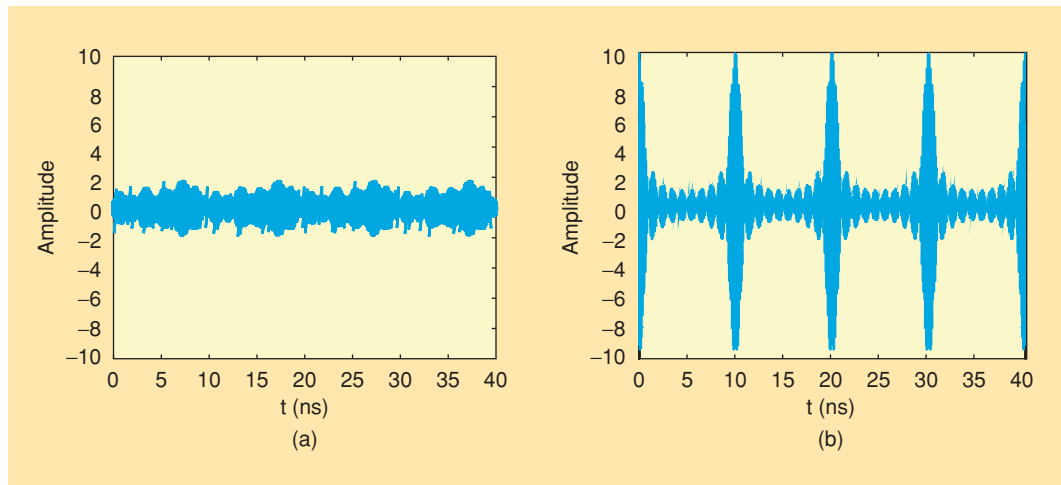

Figure 1. *Time-domain waveforms of two signals composed of ten evenly spaced tones of equal amplitude: (a) independent tones with a randomized phase arrangement and (b) all ten tones phase-locked to a common reference [21].*
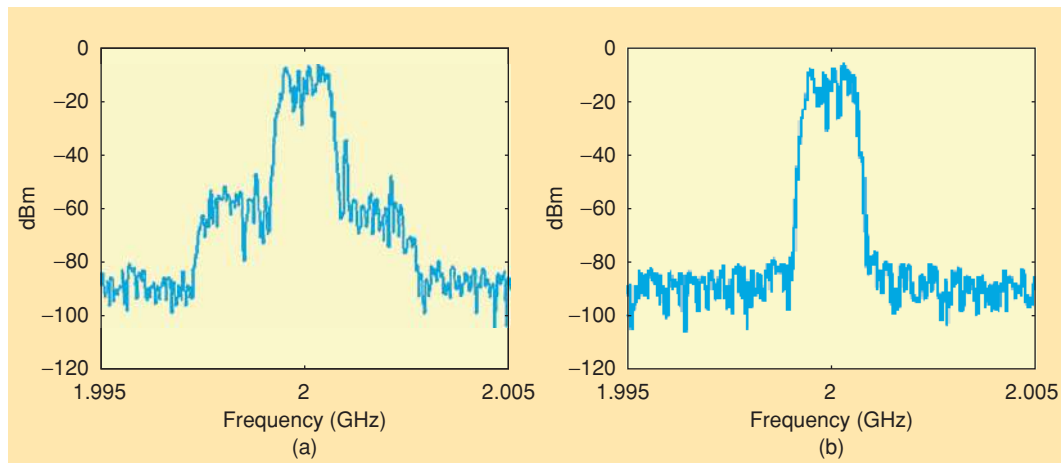

Figure 2. *Measured power spectrum of (a) a CDMA IS95A signal and (b) a 240-tone multisine signal [18].*

This motivates the need to investigate alternative techniques for generating compact multisine representations with the characteristics of practical communication signals for nonlinear circuit analysis. Some of these techniques are based on the statistics of the signal, as discussed in the following section.

Statistical Behavior of Multisines

The response of nonlinear memoryless systems to the excitation's value is instantaneous. So, in principle, we could state that the instantaneous output of such systems is completely determined by the domain of stimulus amplitudes. However, many commonly used system output metrics such as output power, PSD, and adjacent channel power ratio (ACPR) are based on the statistics of a collection of measurements over time. As important as the range of amplitude values covered by the output is, the probability with which they are reached is also fundamental.

This leads us to the intuitive thought that, on average, what matters is not the instantaneous amplitude itself, but the value weighted by the probability density function (PDF) of the signal [19]. For instance, although a very high instantaneous amplitude can determine the signal's amplitude span, the distortion caused by clipping this high-amplitude signal will actually become almost irrelevant to the system's output if it occurs very infrequently.

Thus, while PAPR continues to be an important figure of merit, PDF also plays a key role in the design and verification of bandpass wireless systems. We see this when manufacturers of arbitrary waveform generators (AWGs) start to include information on the PDF or, more commonly, the complementary cumulative distribution function (CCDF) in their equipment.

To help us better understand this problem, several signals of zero mean (zero dc offset) and equal power, but with significantly different PDFs, were selected. Figure 3 presents the PDF(x) of three signals commonly used for model extraction and validation. Here x refers to the voltage value of each sample.

In the figure, one of the signals is an equal-amplitude, two-tone signal. The others are multisines of uniform and Gaussian PDF. The multisines could be used to test a system requiring uniformly or Gaussian-distributed, band-limited white noise waveforms of total power equal to that of the two-tone signal.

There are several ways to synthesize a desired multisine PDF. One useful technique involves an algorithm that automates the procedure of generating a multisine PDF to approximate the PDF of previously synthesized noise sequences [7], [20].

The algorithm functions as follows:

1) Synthesize a noisy signal with the specified PDF statistics pattern and reorder its instantaneous amplitude values in descending order. This creates the vector of PDF bins for the noise.
2) Synthesize an equal-amplitude multisine with the prescribed number and frequency position of tones.
3) Reorder its instantaneous amplitude values in descending order, recording the time samples where they stood. This creates the vector of PDF bins for the multisine.
4) Substitute the amplitudes of the multisine vector of PDF bins by the one for the noise.
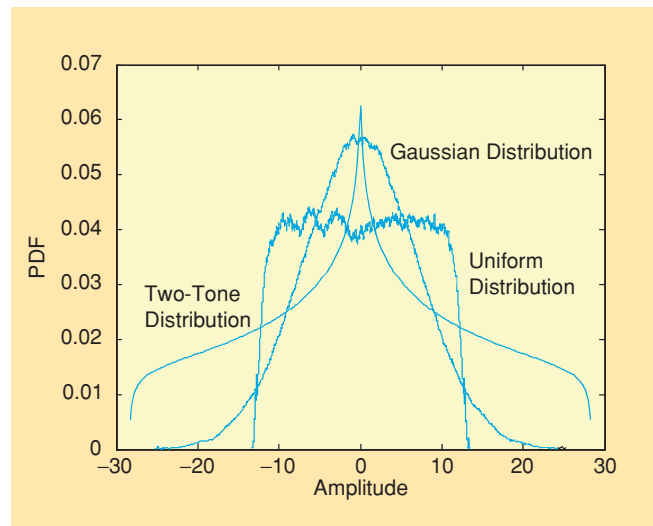5) Restore these amplitudes in the original time samples of the

Figure 3. PDF(x) of a two-tone and two multisines of uniform and Gaussian distribution, all with the same integrated power [21].

multisine, creating a new multisine with the desired PDF.
6) Calculate the DFT of this signal, and level off the resulting tone amplitudes so that the total power is kept, maintaining the phases obtained. This represents the desired multisine we seek.
7) If the process of tone amplitude level-off has modified the multisine PDF to an unacceptable error, repeat the algorithm, using as the starting multisine the one synthesized with this technique, until an acceptably small error is reached.

Figure 4 shows the in-band output obtained by using the two-tone signal and multisines with uniform and Gaussian PDFs to excite a nonlinear memoryless system defined by

$$y(t) = \tanh\left(\frac{x(t)}{20}\right). \tag{4}$$

This memoryless nonlinearity is representative of the nonlinearity found in practical circuits, such as those encountered in power amplifiers.

The integrated value of the nonlinear distortion tones is different for each of the multisine statistics, despite the fact that the input signals had equal amplitudes and number of tones. This implies that a correct description of the signal statistics is fundamental for multisine characterization. "Multisine with Predetermined Higher-Order Statistics" presents the generalization of this problem to higher-order statistics.

Multisine Characterization Figures of Merit

After defining the excitation-signal pattern that can be generated in the laboratory, let us now define some common multisine figures of merit. First of all, let us calculate the output of a polynomial model of a nonlinear amplifier, given in (5), when it is considered memoryless and excited by a continuous signals with PSD $S_{xx}(\omega)$ [21]:

$$y_{NL}(t) = a_1 x(t) + a_2 x(t)^2 + a_3 x(t)^3 + \ldots . \tag{5}$$

From [21], the output will be

$$S_{yy}(\omega) = a_2^2 R_{xx}(0)^2 \delta(\omega) + \Big[a_1^2 + 6a_1 a_3 R_{xx}(0)$$
$$+ 9a_3^2 . R_{xx}(0)^2 \Big] S_{xx}(\omega) + 2a_2^2 S_{xx}(\omega)_* S_{xx}(\omega)$$
$$+ 6a_3^2 S_{xx}(\omega)_* S_{xx}(\omega)_* S_{xx}(\omega) , \qquad (6)$$

where $R_{xx}(0)$ is the autocorrelation function $R_{xx}(t) = E\{x(t)x(t+\tau)\}$ for $\tau = 0$, corresponding to the average power of the input signal. In (6), $\delta(\omega)$ is a Dirac delta function at $\omega = 0$ and $*$ stands for spectral convolution.
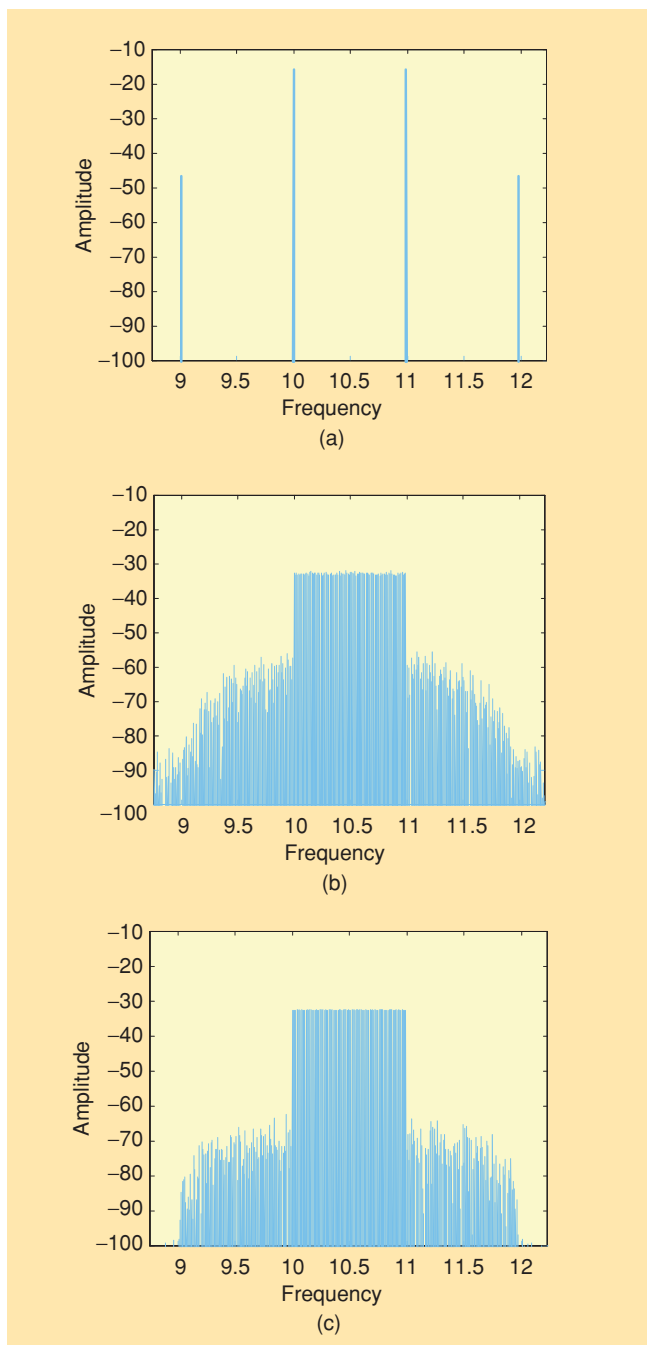

Figure 4. *Output power spectrum of the memoryless system excited by equal power (a) two-tone signal, (b) uniformly distributed, and (c) Gaussian distributed multisines [21].*

A careful look at (6) reveals that different arrangements appear that may allow or prevent us from distinguishing different terms through measurement. For instance, $a_1^2 S_{xx}(\omega)$ (the linear part) and $[6a_1 a_3 R_{xx}(0) + 9a_3^2 R_{xx}(0)^2]S_{xx}(\omega)$ are correlated in phase and appear at the same frequency and thus are indistinguishable from each other. Measurements at these frequencies are normally termed the underlying linear system [3]. The term $6a_3^2 S_{xx}(\omega)_* S_{xx}(\omega)_* S_{xx}(\omega)$ also has components appearing in the in-band zone. The triple convolution is defined in [21]. But these are uncorrelated to the other ones and thus can be distinguished. Understanding these relationships can help us define figures of merit that are appropriate for multisines that mirror those in the wireless world.

The first figure of merit to be presented is the extension from two-tone signals of the intermodulation ratio (IMR). For the case of multisine excitation, this figure of merit is usually called ACPR. This quantity is nothing more than the integrated power of the spectral regrowth due to nonlinear distortion related to the output power, as seen in Figure 5.

Expression (7) represents the multisine-based figure of merit,

$$ACPR_T \equiv \frac{P_o}{P_{LA} + P_{UA}} = \frac{\displaystyle\int_{\omega_{L_2}}^{\omega_{U_1}} S_o(\omega)d\omega}{\displaystyle\int_{\omega_{L_1}}^{\omega_{L_2}} S_o(\omega)d\omega + \displaystyle\int_{\omega_{U_1}}^{\omega_{U_2}} S_o(\omega)d\omega} ,$$

$$(7)$$

where the subscript T denotes integration of power across the entire adjacent channel bandwidth, P_o denotes the total measured output power, P_{LA} and P_{UA} refer to the power in the lower and upper adjacent channels, and ω_U and ω_L are defined in the figure. The ACPR presented in expression (7) is the total integrated power of the spectral regrowth. To better mimic the ACPR defined in some wireless standards, slightly different figures can also be defined as the ACPR, when enough tones exist in the multisine to make this meaningful. This could be done when only one of the sides of the spectral regrowth needs to be accounted for. This may represent only a small part, perhaps 10%, of the frequency bandwidth in the upper or lower spectral regrowth, as given in (8) and Figure 6:
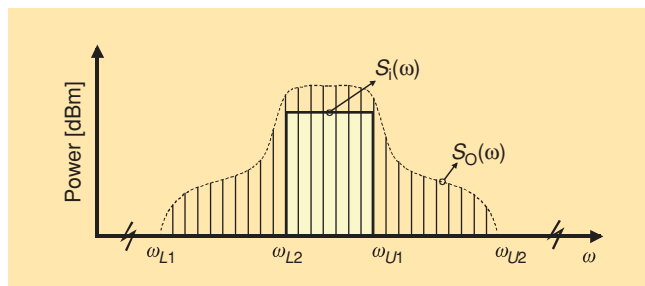

Figure 5. *Input and output power spectra used in the determination of ACPR using multisines. $S_i(\omega)$ is the input PSD and $S_o(\omega)$ is the output PSD [21].*
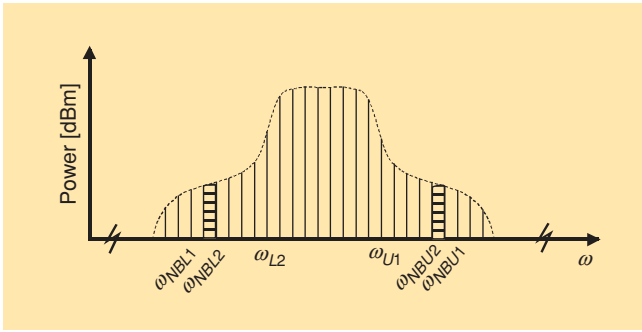
Figure 6. Narrowband ACPR definition [21].

Figure 7. Notch used to measure distortion using NPR [21].

$$ACP_{SP} \equiv \frac{P_o}{P_{SPL/U}} = \begin{cases} \dfrac{\int\limits_{\omega_{L2}}^{\omega_{U1}} S_o(\omega)d\omega}{\int\limits_{\omega_{NBL1}}^{\omega_{NBL2}} S_o(\omega)d\omega} & \text{Lower} \\[2em] \dfrac{\int\limits_{\omega_{L2}}^{\omega_{U1}} S_o(\omega)d\omega}{\int\limits_{\omega_{NBU1}}^{\omega_{NBU2}} S_o(\omega)d\omega} & \text{Upper} \end{cases} \qquad (8)$$

ACPR measurements account exclusively for the spectral regrowth outside the channel, despite the fact that this does not coincide with the useful transmitted signal. It is very difficult to extract the nonlinear distortion that appears exactly over the main channel signal. In order to do this, other figures of merit have been defined, such as noise power ratio (NPR) and cochannel power ratio (CCPR).

In the case of NPR, the idea is to filter from within the excitation signal a notch where the distortion is to be measured (see Figure 7).

The input excitation signal is the same as the real one, but at the notch only the residual thermal noise is visible. At the output, the nonlinear distortion noise will appear at the notch and thus can be measured. The expression for NPR is

$$NPR(\omega_T) \equiv \frac{S_o(\omega_T)}{S_{wd}(\omega_T)}, \qquad (9)$$

where ω_T is the center frequency of the notch, S_o is the output PSD, and S_{wd} is the output PSD within the notch. In this case, we are measuring exclusively the uncorrelated distortion of (6).

In the case of CCPR, the measurement is much more difficult, since no shaping of the input signal is used. In that case, the idea is to eliminate the linear part of the measured output [3] (or the underlying linear system), plus the part of the output distortion that has some correlation with the input signal, as was presented in [22]. Figure 8 presents the overall idea.
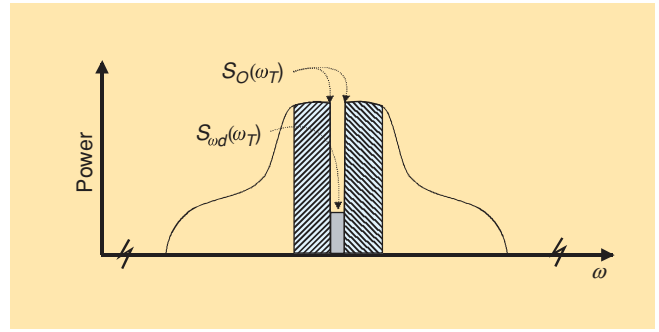
Thus, the CCPR normally represents a figure of merit that eliminates only the linear part of the distortion [22],

$$CCPR \equiv \frac{P_o}{P_{Dcorr}} = \frac{\int\limits_{\omega_{L2}}^{\omega_{U1}} S_o(\omega)d\omega}{\int\limits_{\omega_{L2}}^{\omega_{U1}} S_o(\omega)d\omega - G_{linear}\int\limits_{\omega_{L2}}^{\omega_{U1}} S_i(\omega)d\omega}, \qquad (10)$$

where P_{Dcorr} is the distortion power that has some correlation with the input signal minus the linear part of the distortion, S_o and S_i are the PSDs of the output and input, respectively, and G_{linear} is the linear gain of the device under test (DUT). Additional discussion on CCPR can be found in [22]. The cochannel interference ratio (CIR) [23] stands for the figure of merit that eliminates the underlying linear system,

$$CIR \equiv \frac{P_o}{P_{Dunc}} = \frac{\int\limits_{\omega_{L2}}^{\omega_{U1}} S_o(\omega)d\omega}{\int\limits_{\omega_{L2}}^{\omega_{U1}} S_o(\omega)d\omega - G_{UL}\int\limits_{\omega_{L2}}^{\omega_{U1}} S_i(\omega)d\omega}, \qquad (11)$$

where P_{Dunc} is the distortion power uncorrelated with the input signal and G_{LU} is the underlying linear gain of the DUT.
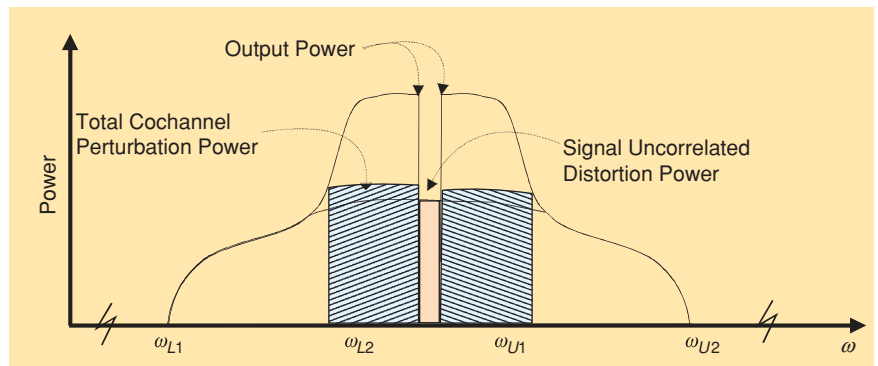

Figure 8. Cochannel distortion [21].

Multisine Measurement Setups

Multisine Signal Generators

Multisine test signals are often synthesized at baseband frequencies by use of an AWG, then up-converted to radio frequency. In fact, many manufacturers sell vector signal generators that are capable of creating multisines directly. Or, a system can be created in-house using phase-locked signal generators and/or an AWG.

In either case, bear in mind that the multisine test signal will not be ideal. Every signal generator is subject to internal distortion, and the stringent requirements placed on the samplers, frequency converters, filters, and other components in the creation of complex modulated signals such as multisines will introduce some degree of distortion. Impedance mismatch can also play a role in altering the desired signal. Characterizing the excitation and understanding the level of impedance mismatch need to be completed before carrying out multisine measurements.

Multisine Receivers

Because multisines contain multiple frequency components, spectral measurements are a convenient way to understand the effects of distortion that is introduced into multisines by a DUT or other system. Measurements with a spectrum analyzer can provide insight into the magnitude of each frequency component.

To gain insight into the phase distortion, we need to measure the relative phase relationships between all frequency components in the signal. For this, instruments that sample time-domain waveforms may be used, such as VSAs [24], LSNAs [16], [17], [25], or sampling oscilloscopes [14]. Or, the spectrum analyzer can be configured with additional instrumentation, as described below. Examples of measurement considerations for these instruments are also described in the following.
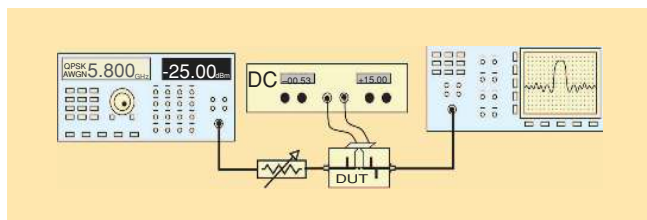

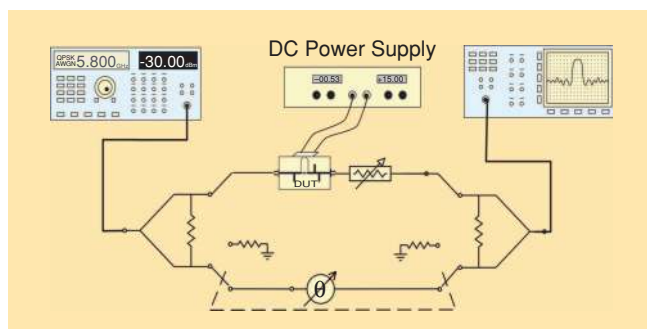**Figure 9.** *Multisine measurement system for ACPR and NPR [21].*

Figure 10. *Cochannel distortion measurement system [21].*

Direct Measurements of Multisines

Spectrum analyzers can directly measure the magnitude of the frequency components in a multisine signal. These instruments are commonly found in the laboratory and are straightforward to use. Because spectrum analyzers sweep across the frequency spectrum, we can extract the power associated with each frequency component in a multisine by integrating across a narrow frequency band containing that component. This typically involves a bit of postprocessing, but it is a fairly straightforward procedure.

VSAs, real-time signal analyzers, and other instruments that rely on downconversion, sampling, and Fourier transformation of the input signal can also easily be used to measure multisine signals. These instruments have some measurement advantages over a spectrum analyzer in acquiring bandpass RF signals. As discussed above, we can acquire both magnitude and phase information directly in each measurement because a time-domain capture is used. These instruments provide a highly sampled, downconverted waveform in order to yield a large amount of spectral detail around the carrier frequency. Using these instruments for acquisition of multisines is fairly straightforward; however, some possible difficulties should be kept in mind.

As with spectrum analyzers, we typically sift through all of the spectral data and use only those frequency components that contribute to the multisine. The power in each frequency component must be found by integration over a band of interest. However, for signal analyzers, methods exist for eliminating spectral leakage [24], thereby ensuring that all of the power in a given frequency component appears at only one frequency. Elimination of spectral leakage negates the need for time-domain filtering (windowing) of the received signal, which is a potential additional source of distortion in the measurement. Multisines lend themselves to these techniques since the sinusoidal frequency components appear only on a fixed grid.

Most VSAs and real-time analyzers have limited modulation bandwidths. Experiments must be designed so that signals in the main channel, as well as the distortion products, are contained within the passband of the instrument, unless a technique such as that of [26] or [27] is utilized to stitch together multiple measurement bands.

Finally, many of these instruments are single channel. To compare the input and output signals directly, multiple measurements must be made. In this case, we can readily lose the phase response of the DUT unless special alignment signals are used, such as those discussed in [28] and [29].

One instrument that is a natural for measuring multisines is the LSNA, sometimes called the nonlinear vector network analyzer. This is a two-port instrument that measures across a limited bandwidth at fundamental and harmonic frequency components. LSNAs maintain phase relationships across the harmonics. The use of postprocessing will also recover the relative phases of the signals measured in the passband [30]. Commercially available LSNAs suffer the same modulation-bandwidth limitation as VSAs and real-time analyzers, but this may change with the advent of mixer-based LSNAs [25].
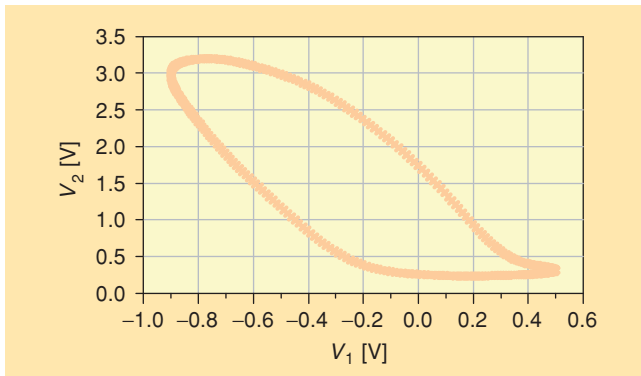
Figure 11. *Trajectory in the (V_1, V_2) plane in the case of a single-tone excitation [32].*

Finally, multisines can also be acquired by the use of a sampling oscilloscope. After transforming to the frequency domain, some postprocessing is needed to extract the power in the desired data frequency components as with some of the other instruments mentioned above. The advantage of the sampling oscilloscope is that it can measure very-wideband modulation bandwidths. One limitation of the oscilloscope is its reduced dynamic range compared to that of the other instruments. Time-domain averaging can overcome this to a certain extent [14]. A comparison of the LSNAs, VSAs, and sampling oscilloscopes in the measurement of multisines is discussed in [14].

Multisine Measurement Bench Using a Spectrum Analyzer for ACPR and NPR

We next discuss a technique whereby a spectrum analyzer and other common test equipment can be used to measure ACPR and NPR by use of multisines. The setup consists of a vector signal generator, a dc bias supply, and a spectrum analyzer, as shown in Figure 9. The generator should be capable of synthesizing the proposed excitation signal.

The proposed setup is able to measure both ACPR and NPR, since the idea in both cases is to measure power over a given bandwidth. Nevertheless, CCPR and CIR are difficult to measure by use of this type of test system. That is the main reason why the test system depicted in Figure 10 is used for this type of measurement [22].

The idea is to mimic the first stage of a feed-forward linearizer, since the objective is to extract the linear contribution from the output signal, in the case of CCPR, or the underlying linear contribution, in the case of CIR. In the case of CCPR, the setup is tuned in the small-signal regime, where the nonlinearity is not so severe, and thus the output can be considered almost linear. In that case, the phase shifter and attenuator are tuned so that the output measured by the spectrum analyzer nulls the cochannel signal. When the input is restored to its desired value, the output is measured based only on the nonlinear part, since the linear one has been eliminated by the lower branch.

For the case of CIR, the idea is to tune the setup exactly at the desired output power of the input signal. In that case, since the lower arm is linear, only the signal components in

the output signal that have some correlation to the input signal will be minimized by the lower arm branch, which is mimicking the lower branch of (11). Thus, the residual signal is the uncorrelated nonlinear contribution of the DUT output signal. We should mention that this minimization is better realized for the case of truly noisy signals. For the case of synchronous multisines, the statistical behavior of the input signal should be carefully taken into account.

Multisine Applications

We have seen in the previous sections how to generate and how to measure multisine signals. In this section, we will see the usefulness of those signals when applied to the simulation of modulated signals and the modeling of nonlinear devices and systems.

For Simulating Modulated Signals

The first application is based on the fact that a multisine can be designed to simulate the statistics of a modulated signal, as explained earlier. Such a multisine can be employed when using measurement instrumentation that cannot handle digitally modulated signals directly, such as an LSNA. This allows for measurements in real-world applications on this type of instrumentation. Practical uses are in testing circuits under realistic operating conditions, as well as using realistic excitations for modeling purposes. An example of the latter can be found in the next section.

For More Efficient Modeling

The second application for multisines is in rendering more efficient the experiment design for behavioral model extraction. We describe a specific application in behavioral modeling approaches that are based on large-signal, time-domain measurement data. Conventionally, such models are extracted from single-tone measurement data. Single-tone excitation is no longer representative of the type of signals to which RF devices are subjected in modern telecommunication systems. Also, many measurements are required for model construction.

To illustrate how multisines can help, the so-called state-space-based modeling approach is considered [31]. In this approach, the dependent variables—typically the port currents—are expressed as a function of the independent variables—typically the port voltages and their higher-order derivatives—up to the higher-order derivatives of the port currents. To ensure good model accuracy over a wide range of experimental conditions, the measurement data used to construct the model must cover the device's state space well. This is a high-dimensional problem that can be illustrated by considering the two-dimensional (2-D) projection on the (V_1, V_2) plane, with V_1 and V_2 being the port voltages of a two-port. Figure 11 shows the (V_1, V_2) trajectory in the case of a single-tone excitation. The data points are on the contour. This graph shows that to cover the (V_1, V_2) plane with sufficient density, a large number of measurements is required.

The number of measurements can be reduced drastically by instead using a multisine excitation [10]. Figure 12 shows the trajectory corresponding to a multisine excitation. In this case, the data points are not only on the contour, but also
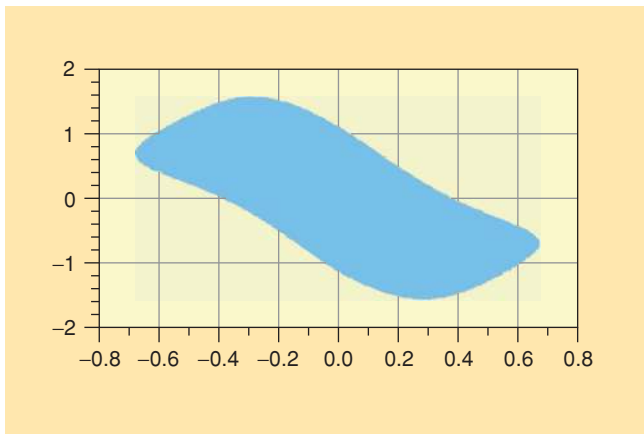
Figure 12. *Trajectory in the (V_1, V_2) plane in the case of a multi-sine excitation [10].*

Figure 13. *PDF of a QPSK-modulated digital signal (solid line) and optimized 63-tone multisine (dotted line) [27].*

densely cover the area within the contour. This can be understood as follows: one trajectory corresponds to one period of the intermediate frequency (IF) envelope. As one IF envelope encompasses thousands of RF periods, the combinations of instantaneous (V_1, V_2) values are much greater. For example, assuming that the fundamental frequency is 1 GHz and the IF period is 40 μs, one IF period encompasses 40,000 RF periods, resulting in at least 800,000 data points (if the number of harmonics considered is ten) when applying the Nyquist theorem. As this number of data points is impractical, subsampling can be performed. This is justified,
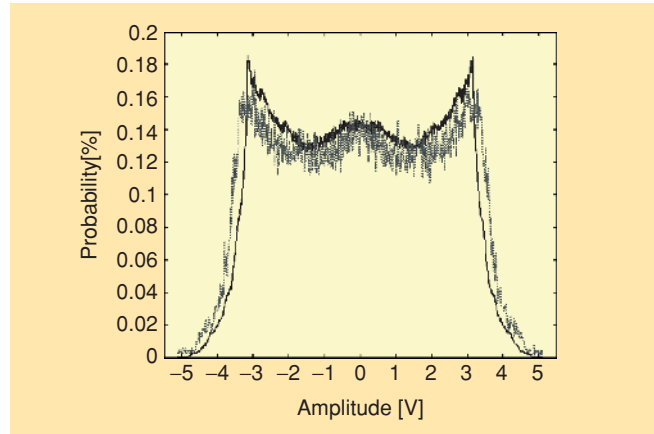
because data points that are neighbors in the state space add little information due to the high density of data points. Various approaches to execute this subsampling have been developed, such as sampling equidistantly in time or according to the degree of nonlinearity [33].

Finally, we show that this approach yields accurate behavioral models. The DUT is a packaged buffer amplifier designed for 4.9-GHz wireless applications. A 63-tone multisine was designed to mimic a 1.6-MHz bandwidth QPSK-modulated digital signal [27]. Figure 13 compares the PDFs of the multisine and the QPSK-modulated digital signal.
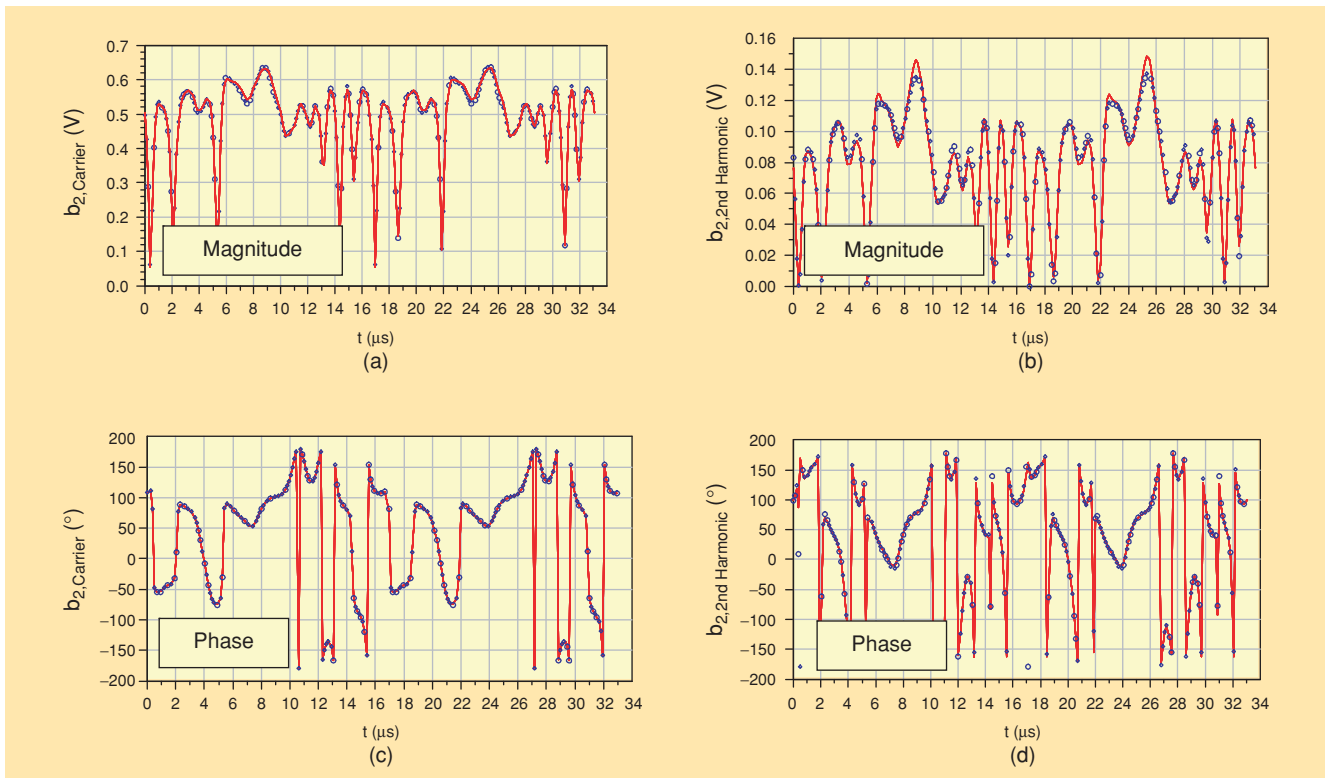

Figure 14. *Measured (circles) and simulated (solid trace) b_2 scattered travelling voltage wave: (a) magnitude waveform, (b) phase waveform of the complex envelope around RF carrier frequency, (c) magnitude waveform, and (d) phase waveform of the complex envelope around the second RF harmonic. The input power is 6 dBm [27].*

After the behavioral model using the multisine measurements was constructed, the model was tested using another set of QPSK-modulated data [27]. The set of plots in Figure 14 depicts the time-domain simulation results (solid trace) together with the corresponding measurements (circles) of the b_2 scattered travelling voltage wave at port 2. The graphs in Figure 14(a) and (b), respectively, show the magnitude and phase of the complex envelope around the carrier frequency. Similar results for the complex envelope around the second RF harmonic are plotted in Figure 14(c) and (d), respectively. We notice very good agreement between the measurements and the model predictions around the RF carrier frequency as well as around its second harmonic.

Conclusions

In summary, we can say that the multisine approach is well suited for evaluating a nonlinear system excited by real communication signals. Multisine signals enable us to gather important information about the in-band distortion and to excite long-term memory effects by generating baseband components. They are periodic and straightforward to characterize, making them ideal for identifying both magnitude and phase distortion during test and verification. Using multisines to simulate standard wireless system excitations and figures of merit allows for very good laboratory nonlinear distortion measurement setups.

Acknowledgments

References

[1] G. Simon and J. Schoukens, "Robust broadband periodic excitation design," *IEEE Trans. Instrum. Meas.*, vol. 49, no. 2, pp. 270–274, Apr. 2000.

[2] J.C. Pedro and N.B. Carvalho, "On the use of multitone techniques for assessing RF components' intermodulation distortion," *IEEE Trans. Microwave Theory Tech.*, vol. 47, no. 12, pp. 2393–2402, Dec. 1999.

[3] R. Pintelon and J. Schoukens, *System Identification: A Frequency Domain Approach*. New York: Wiley-IEEE Press, 2001.

[4] R. Hajji, F. Beauregard, and F.M. Ghannouchi, "Multitone power and intermodulation load-pull characterization of microwave transistors suitable for linear SSPA's design," *IEEE Trans. Microwave Theory Tech.*, vol. 45, no. 7, pp. 1093–1099, July 1997.

[5] K.A. Remley, "Multisine excitation for ACPR measurements," in *2003 IEEE MTT-S Int. Microwave Symp. Dig.*, June 2003, vol. 3, pp. 2141–2144.

[6] K.M. Gharaibeh, K.G. Gard, and M.B. Steer, "In-band distortion of multisines," *IEEE Trans. Microwave Theory Tech.*, vol. 54, no. 8, pp. 3227–3236, Aug. 2006.

[7] J.C. Pedro and N.B. Carvalho, "Designing band-pass multisine excitations for microwave behavioral model identification," in *IEEE MTT-S Int. Microwave Symp. Dig.*, June 2004, vol. 2, pp. 791–794.

[8] W. Van Moer, Y. Rolain, and A. Geens, "Measurement-based nonlinear modeling of spectral regrowth," *IEEE Trans. Instrum. Meas.*, vol. 50, no. 6, pp. 1711–1716, Dec. 2001.

[9] J. Verspecht, F. Verbeyst, and M. vanden Bossche, "Network analysis beyond S-parameters: Characterizing and modeling component behaviour under modulated large-signal operating conditions," in *56th ARFTG Conf. Dig.*, Nov. 2000, pp. 1–4.

[10] D. Schreurs and K.A. Remley, "Use of multisine signals for efficient behavioural modelling of RF circuits with short-memory effects," in *61st ARFTG Conf. Dig.*, Nov. 2003, pp. 65–72.

[11] J.C. Pedro and N.B. Carvalho, "Designing multisine excitations for nonlinear model testing," *IEEE Trans. Microwave Theory Tech.*, vol. 53, no. 1, pp. 45–54, Jan. 2005.

[12] M. Myslinski, K.A. Remley, M.D. McKinley, D. Schreurs, and B. Nauwelaers, "A measurement-based multisine design procedure," in *Proc. Integrated Nonlinear Microwave and Millimeter-Wave Circuits (INMMiC)*, Jan. 2006, pp. 52–55.

[13] W. Van Moer and Y. Rolain, "A multisine based calibration for broadband measurements," in *Proc. IEEE Instrum. Meas. Tech. Conf.*, May 2007, pp. 1–6.

[14] K.A. Remley, P.D. Hale, D.I. Bergman, and D. Keenan, "Comparison of multisine measurements from instrumentation capable of nonlinear system characterization," in *66th ARFTG Conf. Dig.*, Dec. 2005, pp. 34–43.

[15] K.A. Remley, D.F. Williams, D.M.M.-P. Schreurs, and J. Wood, "Simplifying and interpreting two-tone measurements," *IEEE Trans. Microwave Theory Tech.*, vol. 52, no. 11, pp. 2576–2584, Nov. 2004.

[16] M. Demmler, P.J. Tasker, and M. Schlechtweg, "On-wafer large signal power, S-parameter and waveform measurement system," in *Proc. 3rd Int. Workshop on Integrated Nonlinear Microwave and Millimeterwave Circuits (INMMiC)*, 1994, pp. 153–158.

[17] J. Verspecht, P. Debie, A. Barel, and L. Martens, "Accurate on wafer measurement of phase and amplitude of the spectral components of incident and scattered voltage waves at the signal ports of a nonlinear microwave device," in *IEEE MTT-S Int. Microwave Symp. Dig.*, June 1995, vol. 3, pp. 1029–1032.

[18] M. Li, K.M. Gharaibeh, K.G. Gard, and M.B. Steer, "Accurate multisine representation of digital communication signals for characterization of nonlinear circuits," in *Proc. IEEE Radio and Wireless Symp.*, Jan. 2006, pp. 527–530.

[19] J.F. Sevic and M.B. Steer, "On the significance of envelope peak-to-average ratio for estimating the spectral regrowth of an RF/microwave power amplifier," *IEEE Trans. Microwave Theory Tech.*, vol. 48, no. 6, pp. 1068–1071, June 2000.

[20] J. Schoukens and T. Dobrowiecki, "Design of broadband excitation signals with a user imposed power spectrum and amplitude distribution," in *Proc. IEEE Instrumentation and Measurement Technology Conf.*, May 1998, vol. 2, pp. 1002–1005.

[21] J.C. Pedro and N.B. Carvalho, *Intermodulation Distortion in Microwave and Wireless Circuits*. Norwood, MA: Artech House, 2003.

[22] J.C. Pedro and N.B. Carvalho, "Characterizing nonlinear RF circuits for their in-band signal distortion," *IEEE Trans. Instrum. Meas.*, vol. 51, no. 3, pp. 420–426, June 2002.

[23] H. Ku, W. Woo, and J.S. Kenney, "Carrier-to-interference ratio prediction of nonlinear RF devices," *Microwave J.*, vol. 44, no. 2, pp. 154–164, Feb. 2001.

[24] M.D. McKinley, K.A. Remley, M. Myslinski, and J.S. Kenney, "Eliminating FFT artifacts in vector signal analyzer spectra," *Microwave J.*, vol. 49, no. 10, pp. 156–164, Oct. 2006.

[25] P. Blockley, D. Gunyan, and J.B. Scott, "Mixer-based, vector-corrected, vector signal/network analyzer offering 300kHz–20GHz bandwidth and traceable phase response," in *IEEE MTT-S Int. Microwave Symp. Dig.*, June 2005, pp. 1497–1500.

[26] D. Wisell, D. Ronnow, and P. Handel, "A technique to extend the bandwidth of an RF power amplifier test bed," *IEEE Trans. Instrum. Meas.*, vol. 56, no. 4, pp. 1488–1494 Aug. 2007.

[27] M. Myslinski, D. Schreurs, K.A. Remley, M.D. McKinley, and B. Nauwelaers, "Large-signal behavioral model of a packaged RF amplifier based on QPSK-like multisine measurements," in *Proc. European Gallium Arsenide and Other Semiconductor App. Symp. (EGAAS)*, Oct. 2005, pp. 185–188.

[28] M. Myslinski, K.A. Remley, D. Schreurs, and B. Nauwelaers, "RF vector measurement testbench for evaluation of behavioral model accuracy under realistic excitation," in *68th ARFTG Conf. Dig.*, Nov. 2006, pp. 26–31.

[29] J. Hu, K.G. Gard, and N.B. Carvalho, "Dynamic time-frequency waveforms for VSA characterization of PA long-term memory effects," in *Proc. 69th ARFTG Conf.*, June 2007.

[30] K.A. Remley, D.F. Williams, D. Schreurs, G. Loglio, and A. Cidronali, "Phase detrending for measured multisine signals," in *61st ARFTG Conf. Dig.*, 2003, pp. 73–83.

[31] D. Schreurs, J. Wood, N. Tufillaro, L. Barford, and D.E. Root, "Construction of behavioral models for microwave devices from time domain large-signal measurements to speed up high-level design simulations," *Int. J. RF Microwave Computer-Aided Eng.*, vol. 13, no. 1, pp. 54–61, Jan. 2003.

[32] D. Schreurs, M. O'Droma, A. Goacher, and M. Gadringer, *RF Power Amplifier Behavioral Modeling*. Cambridge, U.K.: Cambridge Univ. Press, 2008.

[33] D. Schreurs, K.A. Remley, and D.F. Williams, "A metric for assessing the degree of device nonlinearity and improving experimental design," *IEEE MTT-S Int. Microwave Symp. Dig.*, June 2004, vol. 2, pp. 795–798.